

Analysis of PDZ Domain-Ligand Interactions Using Carboxyl-terminal Phage Display*

Received for publication, January 12, 2000, and in revised form, February 10, 2000

Germaine Fuh, M. Teresa Pisabarro, Ying Li‡, Clifford Quan§, Laurence A. Lasky‡, and Sachdev S. Sidhu¶

From the Departments of Protein Engineering, ‡Molecular Oncology, and §Bioorganic Chemistry, Genentech, Inc., South San Francisco, California 94080

PDZ domains mediate protein-protein interactions at specialized subcellular sites, such as epithelial cell tight junctions and neuronal post-synaptic densities. Because most PDZ domains bind extreme carboxyl-terminal sequences, the phage display method has not been amenable to the study of PDZ domain binding specificities. For the first time, we demonstrate the functional display of a peptide library fused to the carboxyl terminus of the M13 major coat protein. We used this library to analyze carboxyl-terminal peptide recognition by two PDZ domains. For each PDZ domain, the library provided specific ligands with sub-micromolar binding affinities. Synthetic peptides and homology modeling were used to dissect and rationalize the binding interactions. Our results establish carboxyl-terminal phage display as a powerful new method for mapping PDZ domain binding specificity.

PDZ domains, originally described as conserved structural elements in the 95-kDa post-synaptic density protein (PSD-95),¹ the *Drosophila* tumor suppressor discs-large, and the tight junction protein zonula occludens-1 (ZO-1), are contained in a large and diverse set of proteins (1–3). In general, PDZ domain-containing proteins appear to assemble various functional entities, including ion channels and other transmembrane receptors, at specialized subcellular sites such as epithelial cell tight junctions, neuromuscular junctions, and post-synaptic densities of neurons. These clustering and localization effects have important biological implications. For example, the membrane-associated guanylate kinase, PSD-95, segregates the *N*-methyl *D*-aspartate (NMDA) receptor and the Shaker potassium channel to the post-synaptic density of neurons (4). In another illustration, the aggregation of various components of the fruit fly visual system by the multi-PDZ protein INAD greatly enhances the efficiency of this signaling cascade (5). Another compelling case is the use of several PDZ domain-containing proteins in the appropriate basolateral localization of the LET-23 receptor tyrosine kinase of *Caenorhabditis el-*

egans (6). This kinase is required for vulval development, and mutations in these PDZ domain-containing proteins result in the subcellular mislocalization of the LET-23 protein and a lack of vulval differentiation. Together with many other examples, these studies indicate that PDZ domains are important intracellular assembly and localization cofactors in diverse signaling pathways.

PDZ domains recognize three different types of ligands, with two of these interactions showing specificity for peptides at the extreme carboxyl termini of proteins (7–9). Type I and type II PDZ domains recognize carboxyl-terminal peptides with the consensus sequence Thr/Ser-X-Phe/Val/Ala-COOH or Phe/Tyr-X-Phe/Val/Ala-COOH, respectively. Interestingly, a third type of PDZ domain-ligand interaction involves the recognition of an internal peptide sequence. Structural analyses of these three types of PDZ interactions have illuminated the mechanisms of ligand recognition. For example, the crystal structure of a type I PDZ domain from PSD-95 showed that a 4-residue carboxyl-terminal peptide interacts with the protein via an antiparallel main chain association with a β strand, and the terminal carboxylate is inserted into a conserved “carboxylate binding loop” (10, 11). The crystal structure of a PDZ domain from human CASK revealed the nature of interactions mediated by type II motifs (12). In both domain types, the peptide formed a new antiparallel β strand in the PDZ domain structure, and the overall conformations of the two interactions were similar. However, there were significant differences in side chain contacts that could account for the different ligand specificities of the two domain types. Finally, the interaction between a PDZ domain of syntrophin and a PDZ domain of the neuronal nitric oxide synthase has been examined by x-ray and NMR analyses (13, 14). In this case, an extended loop of the neuronal nitric oxide synthase PDZ domain forms a β finger that binds to a β strand of the syntrophin PDZ domain, in a manner that mimics the carboxyl-terminal ligands of types I and II domains. Together, these data suggest that these three types of PDZ domains use similar but highly specialized regions to recognize diverse carboxyl-terminal and internal peptide ligands.

Identification of peptide ligands for novel PDZ domains would advance our understanding of PDZ domain structure and function, and it would also suggest potential functions for these motifs and the proteins that contain them. Initial forays into PDZ domain ligand specificities were performed using combinatorial libraries consisting of either free peptides (15) or peptides fused to the carboxyl terminus of the *Escherichia coli* Lac repressor (16). Although phage display is the most commonly used method for displaying combinatorial peptide libraries, all phage-displayed peptide libraries reported to date have been displayed as fusions to the amino terminus of either the major coat protein (protein-8, P8) or the gene-3 minor coat protein, primarily because it is believed that neither coat pro-

* The costs of publication of this article were defrayed in part by the payment of page charges. This article must therefore be hereby marked “advertisement” in accordance with 18 U.S.C. Section 1734 solely to indicate this fact.

¶ To whom correspondence should be addressed: Dept. of Protein Engineering, Genentech, Inc., 1 DNA Way, South San Francisco, CA 94080. Tel.: 650-225-1056; Fax: 650-225-3574; E-mail: sidhu@gene.com.

¹ The abbreviations used are: PSD-95, post-synaptic density protein; GST, glutathione *S*-transferase; IPTG, isopropylthio- β -*D*-galactoside; MAGI, membrane associated guanylate kinase with inverted orientation; P8, protein-8, the major coat protein of M13 phage; PDZ2 and PDZ3, PDZ domains 2 and 3 of MAGI 3; PSD-95-3, third PDZ domain of PSD-95; ELISA, enzyme-linked immunosorbent assay; BSA, bovine serum albumin; PBS, phosphate-buffered saline.

tein can support carboxyl-terminal fusions (16, 17). Thus phage display has not been used for the display of peptides with free carboxyl termini, and the technology has not been amenable to the analysis of PDZ domain carboxyl-terminal binding specificities (16, 18). Here we demonstrate that P8 can indeed support carboxyl-terminal fusions, and we describe a novel method for the analysis of PDZ domain binding specificities that utilizes this display format. We show that two different PDZ domains from a membrane-associated guanylate kinase select consensus sequences from highly diverse peptide libraries fused to the carboxyl terminus of P8. Synthetic peptides corresponding to the selected sequences bound their cognate PDZ domains with high affinity and specificity, and synthetic peptides were used to determine the binding contributions of individual ligand side chains. We also used molecular modeling to identify putative affinity and specificity determinants on one of these PDZ domains, and we propose possible mechanisms for binding of the selected peptide ligands. Together, these data establish carboxyl-terminal phage display as a powerful new method for mapping PDZ domain ligand specificity.

EXPERIMENTAL PROCEDURES

Materials—Reagents for dideoxynucleotide sequencing were from United States Biochemical Corp. Enzymes and plasmid pMal-p2 were from New England Biolabs. Maxisorp immunoplates were from NUNC (Roskilde, Denmark). *E. coli* XL1-Blue and M13-VCS were from Stratagene. Bovine serum albumin (BSA) and Tween 20 were from Sigma. Streptavidin was from Pierce. Horseradish peroxidase/anti-M13 antibody conjugate, pGEX-4T-3, and glutathione-Sepharose were from Amersham Pharmacia Biotech. Anti-tetra-His antibody was from Qiagen. Anti-GST antibody was from Zymed Laboratories Inc. Horseradish peroxidase/rabbit anti-mouse IgG antibody conjugate was from Jackson ImmunoResearch Laboratories. 3,3',5,5'-Tetramethyl-benzidine/H₂O₂ (TMB) peroxidase substrate was from Kirkegaard & Perry Laboratories Inc.

Peptide Synthesis—Peptides were synthesized using standard 9-fluorenylmethoxycarbonyl (Fmoc) protocols, cleaved off the resin with 2.5% triisopropylsilane in trifluoroacetic acid, and purified by reversed-phase high pressure liquid chromatography. The mass of each peptide was verified by electrospray mass spectrometry.

PDZ Domain Purification—With the full-length MAGI 3 gene as the template, the polymerase chain reaction was used to amplify DNA fragments encoding either PDZ2 (MAGI 3 residues 571–692; forward primer, GATCGATCGTCGACCACACTTGGACTGGTG, and reverse primer, GATCGATCGAGCGGCCGCTATTTCATTTTGGCAG; *SalI* site is in bold and *NotI* site is in bold italics) or PDZ3 (MAGI 3 residues 741–840; forward primer, GGGATCCGTGAAGATAAACACCAACACAC, and reverse primer, GCTCGAGTTTTTCTCCATAGAAGATCT; *BamHI* site is in bold and *XhoI* site is in bold italics). Each amplified fragment was digested with the appropriate restriction enzymes and cloned into a similarly digested pGEX-4T-3 plasmid, resulting in plasmids encoding either GST-PDZ2 or GST-PDZ3 fusion proteins. *E. coli* cultures harboring the appropriate expression plasmids were grown to mid-log phase ($A_{600} = 1.0$) in 1.0 liter of LB broth at 37 °C, induced with 1.0 mM IPTG, and grown for an additional 2 h. The bacteria were pelleted by centrifugation at $4,000 \times g$ for 10 min. The pellet was resuspended in 50 ml of ice-cold PBS and sonicated for 2 min on ice. The suspension was centrifuged for 20 min at $14,000 \times g$, and GST-PDZ fusion proteins were purified from the supernatant by affinity chromatography on 0.5 ml of glutathione-Sepharose.

Vector Construction and Site-directed Mutagenesis—A polymerase chain reaction was performed to amplify a 1.6-kilobase pair fragment of pMal-p2 containing the *lacI^a* gene and a gene fragment encoding the signal peptide from maltose-binding protein under the control of the P_{tac} promoter (forward primer, AAAAGAATTCCCGACACCATCGAATGGTGC, and reverse primer, ACCAGATGCATAAGCCGAGCGGAAAACATCATCG; *EcoRI* site is in bold and *NsiI* site is in bold italics). The DNA fragment was digested with *EcoRI* and *NsiI* and ligated with the large fragment resulting from a similar digestion of a P8 display phagemid (19). The method of Kunkel *et al.* (20) was used to insert eight codons (TAATAACATCACCATCACCATGCG) immediately following the final codon of the P8 open reading frame. The resulting phagemid (designated pS1290a) contained the following DNA sequence downstream of the IPTG-inducible P_{tac} promoter: DNA encoding the

maltose-binding protein signal peptide, mature P8, two stop codons (TAATAA), a penta-His FLAG (HHHHHA), and two more stop codons (TGATAA). Site-directed mutagenesis was used to delete the two stop codons between P8 and the penta-His FLAG or to replace them with varying numbers of Gly codons. The resulting phagemids secreted P8 moieties with carboxyl-terminal fusions consisting of various numbers of Gly residues followed by the penta-His FLAG.

Optimization of the Sequence Linking Peptides to the Carboxyl Terminus of P8—With phagemid pS1290a as the template, a previously described method (21) was used to construct and sort linker libraries that replaced the two stop codons between P8 and the penta-His FLAG with 4, 5, 6, 8, or 10 degenerate codons. The libraries were pooled together to give a total diversity of 1.1×10^{11} . The pool was cycled through rounds of binding selection with an anti-tetra-His antibody as the capture target. After two rounds of binding selection, individual phage were isolated and analyzed in a phage ELISA by capturing the phage with the anti-tetra-His antibody and detecting bound phage (see below). Phage exhibiting strong signals in the phage ELISA were subjected to sequence analysis. The phagemid exhibiting the strongest ELISA signal was designated pS1403a.

Isolation of PDZ-binding Peptides—Phagemid pS1403a was used as a template to construct a library (21) of P8 moieties with carboxyl-terminal fusions consisting of a 13-residue linker (AWEENIDSAPGGG) followed by seven degenerate codons (NNS, where N = A/C/G/T and S = C/G). The diversity of the library was 2.0×10^{10} . The library was cycled through rounds of binding selection with a GST-PDZ fusion protein coated on 96-well Maxisorp immunoplates as the capture target. Phage were propagated in *E. coli* SS320 (21) either with or without 10 μ M IPTG induction. After three or four rounds of binding selection, individual phage were isolated and analyzed in a phage ELISA (see below). Phage that bound to the target GST-PDZ, but not to an unrelated GST-PDZ, were subjected to sequence analysis.

Binding Assays—Binding of peptide-displaying phage particles to immobilized target proteins was detected using a phage ELISA. The assay was performed as described by Pearce *et al.* (22), except that phage were produced in *E. coli* SS320, and assay plates were developed using a TMB peroxidase substrate system (read spectrophotometrically at 450 nm).

The binding affinities of peptides for PDZ domains were determined as IC₅₀ values using competition ELISAs. The IC₅₀ value was defined as the concentration of peptide that blocked 50% of PDZ domain binding to immobilized peptide. Assay plates were prepared by immobilizing amino-terminally biotinylated peptides (ASKVTWV or TRWWFDI for PDZ3 or PDZ4 binding assays, respectively) on maxisorp plates that had been first coated with streptavidin and subsequently blocked with BSA. A fixed concentration of GST-PDZ (60 nM) in PBS, 0.5% BSA, 0.1% Tween 20 (PBT buffer) was preincubated for 3 h with serial dilutions of peptide and then transferred to the assay plates. After 15 min incubation, the plates were washed with PBS, 0.05% Tween 20, incubated with a mixture of anti-GST antibody (0.5 μ g/ml) and horseradish peroxidase/rabbit anti-mouse IgG antibody conjugate (1:2000 dilution) in PBT buffer, washed again, and detected with TMB peroxidase substrate.

Molecular Modeling—The three-dimensional structure of PDZ2 in complex with a high affinity peptide ligand was modeled using homology modeling techniques with the Modeler program (23), based on the coordinates of other PDZ domains solved by x-ray crystallography (Brookhaven Protein Data Bank entry codes 1BE9 and 1PDR) (10, 11). Molecular mechanics calculations to energy-minimize the modeled complex were performed using the cff91 forcefield with the program Discover as implemented in INSIGHTII (23).

RESULTS

Phage Display of Peptides Fused to the Carboxyl Terminus of P8—We constructed a series of phagemids designed to ascertain whether peptides fused to the carboxyl terminus of P8 could be displayed on the surface of M13 phage. Each phagemid was designed to secrete a P8 moiety with a penta-His FLAG epitope (HHHHHA) fused to its carboxyl terminus. Phage particles containing phagemid DNA were produced by co-infecting *E. coli* with the phagemid and a helper phage. In such a system, the majority of the phage coat is composed of P8 molecules supplied by the helper phage (24), but the incorporation of some phagemid-encoded P8 molecules could result in the display of the carboxyl-terminally fused penta-His FLAG. We detected penta-His FLAG display with a phage ELISA using an anti-

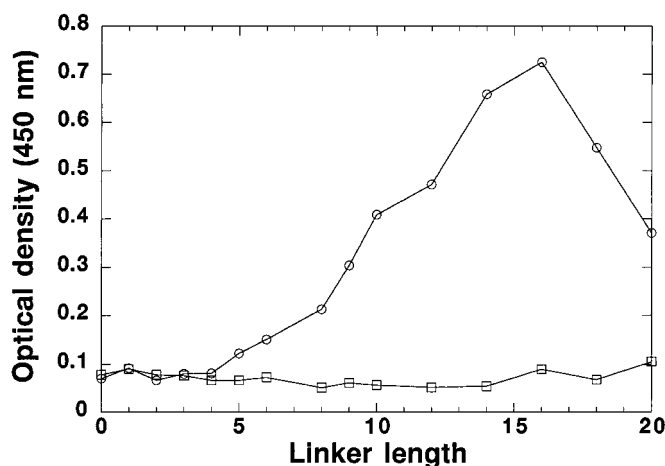


FIG. 1. Phage display of a penta-His FLAG peptide fused to the carboxyl terminus of P8. The FLAG was connected to P8 with intervening polyglycine linkers of varying length. Phage solutions (1.3×10^{12} phage/ml) were incubated in wells coated with an anti-tetra-His antibody to capture phage displaying the penta-His FLAG (circles) or in wells coated with BSA as a negative control (squares). Bound phage were detected in a Phage ELISA. The optical density is proportional to the amount of phage bound and thus measures peptide display levels.

tetra-His antibody as the capture target. Fig. 1 shows that direct fusion of the FLAG to the carboxyl terminus of P8 did not result in display, but display was achieved by inserting five or more Gly residues between the P8 carboxyl terminus and the FLAG. Display levels increased steadily with increasing linker length, reaching a maximum with a 16-residue linker.

To optimize the linker sequence, we constructed libraries in which the linker connecting the penta-His FLAG to the P8 carboxyl terminus was designed to contain 4–6, 8, or 10 randomized residues. The libraries were pooled together and cycled through two rounds of binding selection on plates coated with the anti-tetra-His antibody. Many diverse sequences were selected, but all selectants contained either 8 or 10 residues, again demonstrating a minimum length requirement for the linker. The best linker sequence (AWEENIDSAP) increased display about 10-fold relative to polyglycine linkers of comparable length (data not shown).

Isolation of PDZ Domain Ligands—We constructed a library of random peptides fused to the carboxyl terminus of P8 with an optimized, intervening linker of 13 residues (AWEENID-SAPGGG). At each library position, we used a degenerate codon that encoded all 20 natural amino acids and an amber (TAG) stop codon. The library contained seven degenerate codons and thus predominantly encoded heptapeptides, but the possible occurrence of amber stop codons also provided for the display of shorter peptides. The library contained 2.0×10^{10} unique members and thus exceeded the diversity of all possible natural heptapeptides ($\sim 10^9$).

We used the library to investigate the binding specificities of PDZ domains 2 and 3 (PDZ2 and PDZ3, respectively) of MAGI 3, a membrane-associated guanylate kinase. PDZ2 interacts with the tumor suppressor PTEN/MMAC, whereas the binding specificity of PDZ3 is not known (25). PDZ2 and PDZ3 were purified as glutathione *S*-transferase (GST) fusions from *E. coli*, and the phage-displayed peptide library was cycled through four rounds of binding selection against each domain. Transcription of the phagemid-encoded P8 gene is regulated by the Lac repressor, and display could thus be increased by the addition of IPTG. The PDZ2 sort was successful with or without IPTG, but the PDZ3 sort yielded binding clones only with IPTG induction.

The PDZ2 sort yielded a variety of sequences varying in

TABLE I
Phage-displayed selectants

The sequences were selected after three rounds of sorting with IPTG induction, unless otherwise indicated.

Peptide sequence
PDZ2 binders
DGICSWV ^{a, b}
CSWV ^{b, c}
ASKVTWV ^c
VTWV
EAQCTWV
LEVCSWV
WGPCTWV
PCSWV
IERTTWV
HEEWTVV
GGDCHWV
HKDCHWV
PDZ3 binders
TRWWFDI ^b

^a Isolated without IPTG induction.

^b Represented by multiple clones.

^c Selected after four rounds.

TABLE II

*IC*₅₀ values for PDZ-binding synthetic peptides

The *IC*₅₀ values are the concentrations of peptide that blocked 50% of PDZ domain binding to immobilized peptide in an ELISA.

Position							<i>IC</i> ₅₀	
-6	-5	-4	-3	-2	-1	0	PDZ2	PDZ3
H	T	Q	I	T	K	V ^a	200	NDI ^b
H	T	Q	I	T	W	V	0.3	
D	G	I	C	S	W	V	0.3	NDI
G	G	G	C	S	W	V	2.0	
			C	S	W	V	1.4	
			A	S	W	V	35	
			C	A	W	V	7.3	
			C	S	A	V	200	
			C	S	W	A	400	
A	S	K	V	T	W	V	0.8	NDI
			V	T	W	V	4.0	
T	R	W	W	F	D	I	NDI	0.9
T	R	W	W	F	D	I-NH ₂		300

^a The carboxy-terminal sequence of PTEN/MMAC.

^b NDI indicates no detectable inhibition at peptide concentrations greater than 1 mM.

length from seven to four residues (Table I). The four carboxyl-terminal residues showed a strong consensus to the sequence Cys/Val-Ser/Thr-Trp-Val-COOH, a type 1 PDZ binding consensus related to, but distinctly different from, the carboxyl-terminal sequence of PTEN/MMAC (Tables I and II). Although many of the sequences were represented by unique clones, two carboxyl-terminal sequences appeared multiple times (CSWV and VTWV), both as tetrapeptides and also at the carboxyl termini of longer peptides. Thus, we reasoned that these two sequences represented minimal, high affinity ligands of PDZ2. The PDZ3 sort yielded only a single heptapeptide (TRWWFDI), a type II PDZ-binding motif that differs completely from the PDZ2 binding consensus.

Peptides corresponding to the selected sequences were synthesized and assayed for binding (Table II). The selected peptides bound their cognate PDZ domains with high affinity while exhibiting no detectable binding to non-cognate PDZ domains. Amidation of the carboxyl terminus of the PDZ3-specific peptide resulted in a 300-fold reduction in binding affinity, demonstrating the importance of interactions between PDZ3 and the terminal carboxylate of its ligand. The data also confirmed

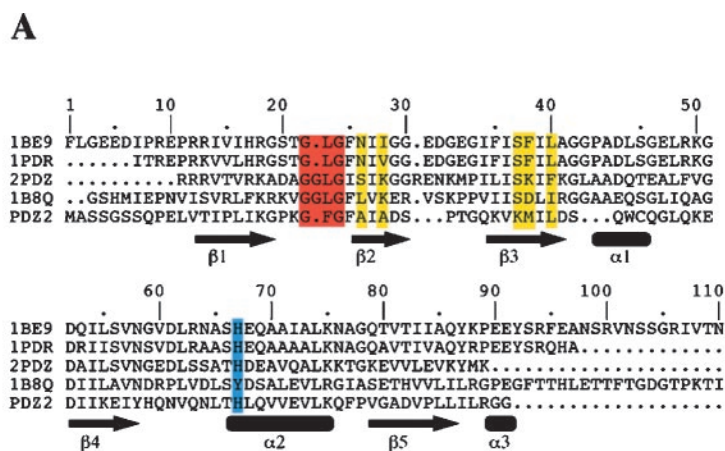
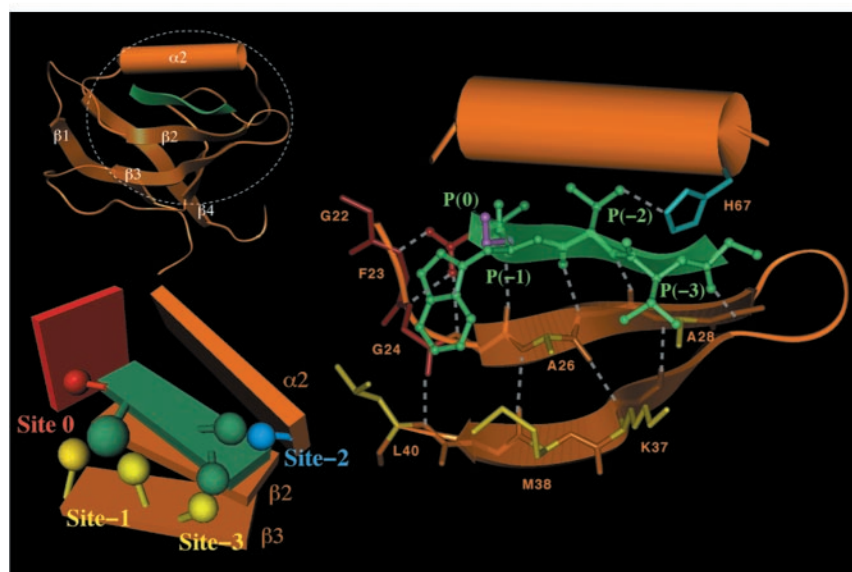
**B**

FIG. 2. Homology modeling of PDZ2 in complex with the high affinity peptide ligand GVTWV. *A*, sequence alignment of PDZ2 with the third PDZ domains of PSD-95 (Protein Data Bank code 1BE9) and the human homologue of discs-large protein (Protein Data Bank code 1PDR), and the PDZ domains of Syntrophin (Protein Data Bank code 2PDZ), and neuronal nitric oxide synthase (Protein Data Bank code 1B8Q). Residues forming the peptide carboxylate binding site (or carboxylate binding loop) are shown in *red*. Residues critical for recognition of peptide side chains at positions P(-1) and P(-3) are shown in *yellow*. The conserved His residue in $\alpha 2$ that hydrogen bonds with Ser/Thr at position P(-2) of the peptide is shown in *blue*. Numbering corresponds to the PDZ2 modeled structure. Secondary structure elements are indicated at the *bottom* of the alignment as *arrows* (β strand) and *rectangles* (α helix). *B*, the homology model. *Top left*, ribbon representation of the modeled PDZ2/GVTWV complex. The protein is shown in *orange*, and the peptide ligand in *green*. The secondary structural elements are labeled. The *dashed ellipse* shows the area zoomed in. *Right*, zoom in of $\beta 2$, $\beta 3$, $\alpha 2$ and the peptide ligand. The peptide side chains are shown in a *ball and stick* representation; P(0) is in *red*, and P(-1), P(-2) and P(-3) are in *green*. For comparison at P(-1), the Ser side chain of the ligand in the PSD-95-3/KQTSV crystal structure is shown in *magenta*. The color code for the PDZ domain is the same as in the sequence alignment. Hydrogen bonds are shown as *white dashed lines*. Some protein side chains have been omitted for clarity. *Bottom left*, schematic view of the PDZ domain binding sites for each of the four residues in a tetrapeptide ligand. In addition to previously described interactions with the residues at P(0) and P(-2), the schematic also depicts proposed interactions between the peptide side chains at P(-1) and P(-3) and PDZ side chains in the $\beta 3$ strand.

that the minimal tetrapeptide selectants from the PDZ2 sort bind PDZ2 with high affinity. Surprisingly, the selectants bound PDZ2 much more tightly than a heptapeptide corresponding to the carboxyl-terminal sequence of PTEN/MMAC. It appears that this large difference in binding affinity is entirely attributable to the residue at P(-1),² which is a Trp in the selected peptide as opposed to a Lys in PTEN/MMAC (compare HTQITWV with HTQITKV, Table II).

To assess the contributions of individual ligand side chains to the binding interaction, the tetrapeptide exhibiting the high-

est affinity for PDZ2 (CSWV) was subjected to an alanine scan. A peptide series was synthesized to convert individually each amino acid within the tetrapeptide to an Ala residue. The results indicate that all four side chains contribute favorably to the binding interaction (Table II), but the magnitudes of the contributions vary. Ala substitution at P(0) or P(-1) reduced binding by more than 100-fold, whereas substitution of the serine residue at P(-2) caused only a 5-fold reduction. Ala substitution of the cysteine residue at P(-3) caused an intermediate 25-fold reduction in binding.

Modeling the PDZ2-Peptide Interaction—We used homology modeling techniques to build a three-dimensional model of PDZ2 in complex with the high affinity pentapeptide ligand GVTWV (Figs. 2 and 3). The model was based on the crystal

² Positions in the peptide ligand, from the carboxyl terminus to the amino terminus, are designated P(0), P(-1), P(-2), etc. The corresponding binding sites on PDZ domains are designated site(0), site(-1), site(-2), etc.

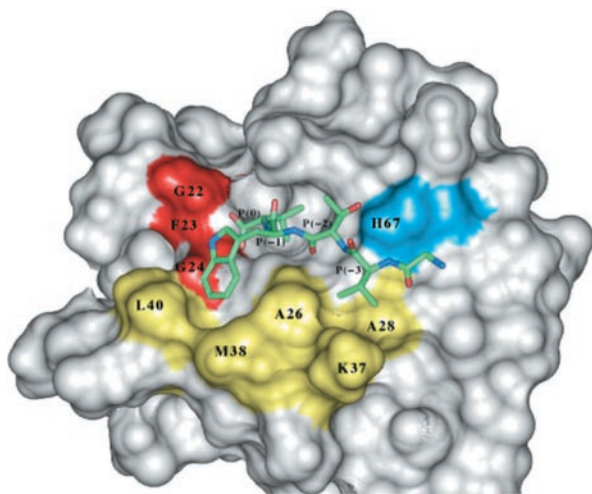


FIG. 3. Molecular surface of the modeled PDZ2-GVTWV complex. Protein residues conferring binding affinity and/or specificity are shown in color. The color code is the same as in Fig. 2; the carboxylate binding loop is *red*; residues in $\beta 2$ and $\beta 3$ that interact with peptide side chains at P(-1) and P(-3) are *yellow*, and the conserved His side chain that hydrogen bonds with the Ser/Thr at P(-2) is *blue*.

structures of the third PDZ domain from the human homolog of discs-large protein (11) and the third PDZ domain of PSD-95 (PSD-95-3) in complex with a pentapeptide (KQTSV) (10). The model and the peptide alanine scan data help to define the binding interactions between PDZ2 and peptide ligands. In both the crystal structure and the model, the peptide ligand forms a β strand that intercalates between $\beta 2$ and $\alpha 2$ of the PDZ domain, extending the antiparallel β sheet formed by $\beta 2$ and $\beta 3$ of the protein (Fig. 2). The terminal carboxylate of the peptide interacts with the highly conserved carboxylate binding loop (main chain of residues Gly-22, Phe-23, and Gly-24), whereas the P(0) Val side chain resides in a well defined hydrophobic pocket. In the PSD-95-3/KQTSV crystal structure, the side chain of Ser at P(-1) is solvent-exposed, and it does not interact with the protein (Fig. 2). Thus, the P(-1) side chain in PDZ domain ligands has been considered unimportant for binding, and the type I consensus sequence X-Ser/Thr-X-Val-COOH has been proposed (10). In contrast, the bulky Trp side chain at P(-1) of our high affinity ligands can be modeled to pack against the protein (Fig. 2), establishing favorable Van der Waals contacts with the side chains of Met-38 and Leu-40 in the $\beta 3$ strand (Fig. 3). These interactions would bury a large hydrophobic area and greatly stabilize the complex. This prediction is supported by the dramatic reduction in binding upon substitution of Trp with Ala at P(-1) (Table II). Met-38 and Leu-40 are not conserved in the PDZ family (Fig. 2A), indicating that interactions between side chains at these positions and peptide side chains at P(-1) may contribute not only to binding affinity but also to specificity. At P(-2), the Thr side chain makes a hydrogen bond to the conserved His-67 residue in both the crystal structure and the model (Fig. 2). However, the interaction is solvent-exposed, and Ala substitution at this position has only a modest effect on affinity (Table II). Thus, the side chain at P(-2) may determine specificity, but it makes only a minor contribution to affinity in the case of PDZ2 binding to the selected peptides. Finally, the binding contribution of the hydrophobic side chain at P(-3) can be rationalized in terms of favorable Van der Waals contacts with a hydrophobic patch on the protein formed by the side chains of residues Ala-26 and Ala-28 in the $\beta 2$ strand and the side chain of Lys-37 in the $\beta 3$ strand (Figs. 2 and 3). Our results confirm the importance of the previously described interactions between the carboxyl terminus of the peptide ligand and the carboxylate

binding loop of the PDZ domain. In addition, our data highlight contributions to binding affinity and specificity attributable to interactions between hydrophobic side chains at P(-1) and P(-3) of the peptide ligand and side chains in the $\beta 2$ and $\beta 3$ strands of the PDZ domain.

DISCUSSION

Phage-displayed peptide libraries fused to the amino terminus of P8 have proven to be a rich source of highly specific ligands (21), but it is widely believed that fusions to the carboxyl terminus of P8 cannot be displayed (16, 17). This belief is based on structures of filamentous phage determined by x-ray fiber diffraction, because these structures indicate that the P8 amino terminus is solvent-exposed, whereas the carboxyl terminus is buried in the core of the particle (26). However, the structure also reveals that the phage coat is essentially a repeating array of several thousand P8 molecules, and we reasoned that a few P8 molecules with carboxyl-terminal fusions may be tolerated in a coat predominantly composed of wild-type P8. Our results clearly demonstrate the viability of carboxyl-terminal P8 fusions in a phagemid system, where the majority of the coat is wild-type P8 supplied by a helper phage (24). The fact that display is dependent on linker length is consistent with a minimum peptide length necessary to extend the carboxyl terminus from the core of the phage particle to the solvent-exposed surface. Any phagemid-based system can be adapted for carboxyl-terminal P8 display, since all aspects of the format are analogous to conventional phage display. For example, display levels were increased by IPTG induction of a regulated promoter, and standard phage display selection methods worked well with the new format. Library members containing stop codons are not displayed as amino-terminal fusions, but in the carboxyl-terminal display format, random stop codons actually expanded library diversity by producing truncated peptides that were displayed (Table I).

The perceived limitations of phage display prompted Cull *et al.* to develop an elegant alternative (27). Their "peptides-on-plasmids" technique enabled the display of peptide libraries with free carboxyl termini, because the libraries were fused to the carboxyl terminus of the *E. coli* Lac repressor that in turn bound tightly to the peptide-encoding plasmid. The plasmid and phage display methods are analogous in principle, but they differ significantly in the requirements for library purification and propagation. M13 phage particles are secreted directly into the media, and a simple precipitation can be used to purify the phage away from the *E. coli* host and most host proteins (21). In contrast, peptide-plasmid complexes are obtained in bacterial lysates and thus remain associated with soluble *E. coli* proteins (16). Following rounds of binding selection, phage particles can be efficiently propagated by infection of an appropriate host strain. The introduction of plasmids into host cells requires less efficient and more complicated transformation procedures (16). Whatever the particular method, carboxyl-terminal display formats open up new applications unsuitable for amino-terminal display. These include the display of cDNA libraries in which natural stop codons limit amino-terminal display (17) and also the PDZ domain binding specificity analyses reported here.

An interesting result from our studies is the fact that phage-selected peptides actually bind PDZ2 more tightly than a peptide corresponding to the carboxyl-terminal sequence of a natural PDZ2 ligand, the tumor suppressor PTEN/MMAC (Table II). The selected consensus sequence is similar to the PTEN/MMAC sequence in three of the four carboxyl-terminal positions, but a major difference between the two sequences is found at P(-1), where the PTEN/MMAC sequence contains a Lys, whereas the selected sequence contains a Trp. This Trp side chain is critical for high affinity binding (Table II), and

molecular modeling studies suggest that it makes highly specific Van der Waals contacts with the PDZ domain (Figs. 2 and 3). These results suggest that PDZ2 is capable of binding to both low and high affinity ligands, with the P(-1) side chain determining the affinity of the interaction. Protein data base searches (28) for the Ser/Thr-Trp-Val-COOH motif revealed that an epithelial cell junction protein, δ -catenin, ends in this sequence (data not shown). The possibility that δ -catenin may tightly interact with MAGI proteins is interesting, because catenins appear to be localized to the tight junctions of epithelial cells by an unknown mechanism. One interpretation of these data is that PDZ2 interacts with high affinity ligands, such as catenins, for subcellular localization and also with low affinity ligands, such as PTEN/MMAC, for the control of cell signaling.

Structural studies have revealed that the peptide ligand forms an additional β strand in the PDZ domain structure through main chain interactions with β 2 (10). In addition to previously noted interactions, our results highlight the binding contributions of peptide side chains at P(-1) and P(-3) (Table II). Our modeling studies suggest that side chains at these positions reach across β 2 and make specific contacts with side chains in β 3 (Figs. 2 and 3). These interactions help to explain PDZ domain binding specificity and affinity, and it is notable that similar " β 1- β 3" interactions between hydrophobic side chains have been found to stabilize three-stranded antiparallel β sheet proteins such as WW domains (29). In fact, such β 1- β 3 interactions have been used to drive β sheet formation in *de novo* protein design experiments (30). The PDZ domain side chains involved in these interactions are not conserved in the PDZ family, and thus, such interactions could be used to introduce both affinity and specificity in designed PDZ domain ligands.

REFERENCES

1. Tsunoda, S., Sierralta, J. & Zuker, C. (1991) *Curr. Opin. Genet. & Dev.* **8**, 419–422
2. Craven, S. & Brecht, D. (1998) *Cell* **93**, 495–498
3. Fanning, A. & Anderson, J. (1999) *J. Clin. Invest.* **103**, 767–772
4. Tejedor, F., Bokhari, A., Rogero, O., Gorczyca, M., Zhang, J., Kim, E., Sheng, M. & Budnik, V. (1997) *J. Neurosci.* **17**, 152–159
5. Tsunoda, S., Sierralta, J., Sun, Y., Bodner, R., Suzuki, E., Becker, A., Socolich, M. & Zuker, C. (1997) *Nature* **388**, 243–249
6. Kaech, S., Whitfield, C. & Kim, S. (1998) *Cell* **94**, 761–771
7. Cowburn, D. (1997) *Curr. Opin. Struct. Biol.* **7**, 835–838
8. Harrison, S. (1996) *Cell* **86**, 341–343
9. Oschkinat, H. (1999) *Nat. Struct. Biol.* **6**, 408–410
10. Doyle, D., Lee, A., Lewis, J., Kim, E., Sheng, M. & Mackinnon, R. (1996) *Cell* **85**, 1067–1076
11. Morais-Cabral, J., Petosa, C., Sutcliffe, M., Raza, S., Byron, O., Poy, F., Marfatia, S., Chisti, A. & Liddington, R. (1996) *Nature* **382**, 649–652
12. Daniels, D., Cohen, A., Anderson, J. & Brunger, A. (1998) *Nat. Struct. Biol.* **5**, 317–325
13. Hiller, B., Christopherson, K., Prehoda, K., Brecht, D. & Lim, W. (1999) *Science* **284**, 812–815
14. Tochio, H., Zhang, Q., Mandal, P., Li, M. & Zhang, M. (1999) *Nat. Struct. Biol.* **6**, 417–421
15. Songyang, Z., Fanning, A. S., Fu, C., Xu, J., Marfatia, S. M., Chisti, A. H., Crompton, A., Chan, A. C., Anderson, J. M., and Cantley, L. C. (1997) *Science* **275**, 73–77
16. Strickler, N., Christopherson, K., Yi, B., Schatz, P., Raab, R., Dawes, G., Bassett, D., Brecht, D. & Li, M. (1997) *Nat. Biotechnol.* **15**, 336–342
17. Palzkill, T., Huang, W. & Weinstock, G. (1998) *Gene (Amst.)* **221**, 79–83
18. Gee, S., Sekely, S., Lombardo, C., Kurakin, A., Froehner, S. & Kay, B. (1998) *J. Biol. Chem.* **273**, 21980–21987
19. Lowman, H., Chen, Y., Skelton, N., Mortenson, D., Tomlinson, E., Sadick, M., Robinson, I. & Clark, R. (1998) *Biochemistry* **37**, 8870–8878
20. Kunkel, T., Roberts, J. & Zakour, R. (1987) *Methods Enzymol.* **154**, 367–382
21. Sidhu, S., Lowman, H., Cunningham, B. & Wells, J. (2000) *Methods Enzymol.*, in press
22. Pearce, K., Jr., Potts, B., Presta, L., Bald, L., Fendly, B. & Wells, J. (1997) *J. Biol. Chem.* **272**, 20595–20602
23. Molecular Simulations, Inc. (1999) *Insight II*, Molecular Simulations, Inc., San Diego
24. Wilson, D. & Findlay, R. (1998) *Can. J. Microbiol.* **44**, 313–329
25. Wu, Y., Dowbenko, D., Spencer, S., Laura, R., Lee, J., Gu, Q. & Lasky, L. (2000) *J. Biol. Chem.* **275**, 21477–21485
26. Marvin, D. (1998) *Curr. Opin. Struct. Biol.* **8**, 150–158
27. Cull, M., Miller, J. & Schatz, P. (1992) *Proc. Natl. Acad. Sci. U. S. A.* **89**, 1865–1869
28. Hofmann, K., Bucher, P., Falquet, L. & Bairoch, A. (1999) *Nucleic Acids Res.* **27**, 215–219
29. Macias, M., Hyvonen, M., Baraldi, E., Schultz, M., Sudol, M., Saraste, M. & Oschkinat, M. (1996) *Nature* **382**, 646–649
30. Kortemme, T., Ramirez-Alvarado, M. & Serrano, L. (1998) *Science* **281**, 253–256